OPTIK 127 (2016) 9738–9742

Contents lists available at ScienceDirect

Optik

journal homepage: www.elesevier.de/ijleo

Optical Single Carrier-Interleaved Frequency Division Multiplexing for Visible Light Communication Systems

Osama Said [a], Zabih Ghassemlooy [b], Sujan Rajbhandari [c] and Andrew Burton [b]

[a]*Department of Electrical and Electronic Engineering, University of Gharyan, Gharyan, Libya, osama.dhawi.saied@hotmail.com*
[b]*Optical Communications Research Group, Faculty of Engineering and Environment, Northumbria University, Newcastle Upon Tyne, NE1 8ST, UK, {z.ghassemlooy, andrew2.burton}s@northumbria.ac.uk*
[c] *Institute for Future Transport and Cities, School of Computing, Electronics and Mathematics, Coventry University, Coventry, CV1 5FB, UK, ac1378@coventry.ac.uk*

* *Corresponding author.*Osama Saied.
E-mail address: osama.dhawi.saied@hotmail.com

ARTICLE INFO

Article history:
Received dd mm 2019
Accepted dd mm 2019

Keywords:
SC-IFDMA; PAPR; visible light communications

ABSTRACT

In this paper, a novel optical single carrier-interleaved frequency division multiplexing (OSC-IFDM) signaling scheme for an intensity modulation and direct detection (IM/DD) based visible light communications (VLC) system is presented. We show that, OSC-IFDM significantly improves the peak-to-average-power ratio (PAPR) of the DC-biased optical orthogonal frequency division multiplexing (DCO-OFDM). The reduction in the PAPR value is achieved by exploiting the symmetrical characteristics of the single carrier-interleaved frequency division multiple access (SC-IFDMA) time domain symbol, whereby the imaginary and real parts of the SC-IFDMA samples are separated and transmitted through two sub-symbols. Simulation results show that, the PAPR of OSC-IFDM is 10 dB lower than that of the DCO-OFDM scheme. We also show that the proposed scheme offers higher spectral efficiency compared to our previous work.

1. Introduction

Visible light communications (VLC) refers to a wireless technology, which utilizes white light emitting diodes (LEDs) for illumination, data transmission and localization. VLC systems are cost-effective, energy efficient and highly secure. Furthermore, VLC occupies the unlicensed portion of the electromagnetic spectrum and offers a very large transmission bandwidth (BW) in comparison to the RF spectrum [1-3]. However, the standard high power white phosphor light emitting diodes (WPLED) used for illumination have a limited modulation BW (typically a few MHz [1, 2]), which limits the maximum data rates that can be achieved. To overcome the WPLED bandwidth limitation, blue optical filters are used to remove the slow temporal response of the phosphor at the receiver [4]. In addition to blue filtering, pre- and post-equalization schemes as well as multi-level modulation techniques have been shown to significantly improve the achievable data rate [5]. However, these techniques cause a reduction in signal power, which reduces the signal-to-noise ratio (SNR) [2, 6]. Recently, spectrally efficient orthogonal frequency division multiplexing (OFDM) with bit and power-loading have been demonstrated to offer transmission data rates close to the Shannon limit, achieving a data rate of >10 Gb/s using red, green and blue (RGB) LEDs [7].

For intensity modulation and direct detection (IM/DD) based VLCs, the modulating signals must be non-negative and real. As a result, complex and bipolar signal formats such as the traditional OFDM cannot be used [2, 8]. Hence, modifications to the traditional OFDM have been proposed for IM/DD

VLC systems, which include DC-biased optical OFDM (DCO-OFDM) and asymmetrically clipped optical OFDM (ACO-OFDM). In these schemes, Hermitian symmetry (HS) is imposed prior to the inverse fast Fourier transform (IFFT) operation to achieve a real time-domain signal at the cost of reduced spectral efficiency by up to 50%. Furthermore, to ensure that the signal is non-negative, a DC-bias is added prior to clipping the negative residual signals in DCO-OFDM. In the ACO-OFDM scheme, only the odd subcarriers are used to carry data to ensure an asymmetrical time domain signal with real and positive values. As such, DCO-OFDM has a higher spectral efficiency whilst ACO-OFDM offers improved power efficiency [9, 10].

Owing to the high peak-to-average-power ratio (PAPR) of the OFDM signal, its generation can be adversely affected by the non-linear distortion arising from the limited dynamic range of LED's power-current characteristics, electrical post-amplifiers or the limited digital-to-analogue converter dynamic range (DACDR) [2, 11]. In VLC systems, a signal that exceeds the LED's linear range will experience non-linear distortion, which negatively affects the bit error rate (BER) performance and the diming control feature [1, 2]. In order to reduce the PAPR, a single carrier-interleaved frequency division multiple access (SC-IFDMA) scheme was investigated [12-14]. However, SC-IFDMA for an IM/DD-based VLC system requires a HS process in order to ensure a real-value signal. This makes the PAPR value of the optical SC-IFDMA higher than that of SC-IFDMA in the RF domain. It was shown in [14] that, only half of the modified SC-IFDMA samples will have a single carrier behavior, while the other half will have a PAPR similar to OFDM.

In our recent work [15], the PAPR of an optical OFDM signal was significantly reduced for IM/DD based VLC systems by employing SC-IFDMA with no HS. This was achieved by repeating the SC-IFDMA time domain symbol symmetrically four times through setting the interleaving factor (Q) in the frequency domain to four. As such, the SC-IFDMA symbol is transmitted using the 1st, 2nd, 3rd and 4th sub-symbols, which represent positive values of the real and imaginary samples, and negative values of real and imaginary samples, respectively. However, the 1st subcarrier (DC-bias) in [15] was none-zero (i.e., modulated subcarrier), which can affect all time domain samples and consequently increase the BER. Note that, the DC-bias is a requirement in VLC systems for illumination and to remove the effect of the pulse shaping filter, which can convert unipolar signals into a bipolar format [1, 2, 16]. In order to improve the performance of our aforementioned work in [15], we have introduced a dedicated algorithm to reduce the effect of the DC-bias, but at the cost of increased SNR compared to the traditional DCO-OFDM. Furthermore, we show that, the spectral efficiency is doubled by reducing Q by a factor of 2 compared to the previous work [15].

The rest of the paper is structured as follows; Section 2 presents the proposed optical single carrier-interleaved frequency division multiplexing (OSC-IFDM) scheme, while the DC-bias noise reduction algorithm is discussed in Section 3. The results obtained for the proposed scheme are analyzed and evaluated in Section 4. Finally, conclusions are drawn in Section 5.

2. Optical Single Carrier-Interleaved Frequency Division Multiplexing (OSC-IFDM)

In this section, an analysis of the proposed OSC-IFDM system, as well as full descriptions of the transmitter (Tx) and the receiver (Rx) structures, are presented. Furthermore, the interleaving mapping technique is investigated to make SC-IFDMA applicable for IM/DD VLC systems.

2.1. OSC-IFDM transmitter

Fig. 1 depicts the block diagram of the OSC-IFDM Tx, which is similar to the Tx used in the standard SC-IFDMA scheme [17]. The main differences are the inclusion of the intensity modulation process (IMP) and intensity demodulation process (IDMP) blocks at the Tx and the Rx of OSC-IFDM, respectively. The signal processing steps at the Tx can be described as follows. First, the serial binary bits b_i stream is converted into parallel data streams and mapped onto a group of complex quadrature amplitude modulation (QAM) symbols $\bar{x}$, as given by:

$$\bar{x} = [\bar{x}_0, \bar{x}_1, \bar{x}_2, \dots \bar{x}_{M-1}], \tag{1}$$

where $\bar{x}_0, \bar{x}_1, \bar{x}_2, \dots \bar{x}_{M-1}$ refer to the k^{th} complex QAM symbol, and M is the number of data symbols. Note that, as will be explained in detail in Section 3, to reduce the DC-bias induced noise, the first symbol in $\bar{x}$ is unmodulated (i.e., $\bar{x}_0 = 0$). The complex symbols are transformed to the frequency domain by applying a fast Fourier transform (FFT) operation. The output in the frequency domain is given by:

$$\bar{X}_m = \sum_{k=0}^{M-1} \bar{x}_k \ \mathrm{e}^{-j2\Pi \frac{k}{M} m}, \tag{2}$$

where $\bar{X}_m$ refers to the m^{th} subcarrier, $m = \{0,1,2, \dots . M-1\}$ and $\bar{X} = [\bar{X}_0\ \bar{X}_1, \overline{X_2} \cdots \bar{X}_{M-1}] \in \mathbb{C}^M$ denotes the set of M-dimensional complex numbers. The interleaving mapping is carried out on $\bar{X}$ by inserting (Q-1) number of zeros between the adjacent subcarriers (here Q = 2, see Fig. 1). The mapped output signal is defined as:

$$X_i = \begin{cases} \bar{X}_m, & \text{if } i = Qm \text{ where } 0 \le m \le M-1 \\ 0, & \text{otherwise} \end{cases} \tag{3}$$

where $i = \{0,1,2, \dots . N-1\}$, $X = [X_0, X_1, X_2, \dots . . X_{N-1}]$ and $N = QM$.

The mapped frequency domain signal is then converted back into the time domain signal as given by:

$$x_n = \frac{1}{N}\sum_{i=0}^{N-1} X_i \, e^{j2\Pi \frac{i}{N} n}, \tag{4}$$

where x_n refers to the n^{th} time domain sample, $n = \{0,1,2,\ldots . N-1\}$ and $x = [x_0\, x_1, x_2 \cdots x_{N-1}] \in \mathbb{C}^N$ following the interleaving process. Let: $n = (Mq + m)$ for $0 \le q \le Q-1$ in (4), then we obtain [17]:

$$\begin{aligned} x_n &= x_{Mq+m} \\ &= \frac{1}{N}\sum_{i=0}^{N-1} X_i \, e^{j2\Pi \frac{i}{N}(Mq+m)} \\ &= \frac{1}{Q}\frac{1}{M}\sum_{i=0}^{M-1} X_m \, e^{j2\Pi \frac{k}{M} m} \\ &= \frac{1}{Q}\left[\frac{1}{M}\sum_{i=0}^{M-1} X_m \, e^{j2\Pi \frac{k}{M} m}\right] \\ &= \frac{1}{Q}\bar{x}_k. \end{aligned} \tag{5}$$

From (5), it can be clearly seen that x_n is the scaled (in amplitude) version of $\bar{x}_k$ and has the characteristics of a single carrier with a low PAPR. However, due to the interleaving mapping of $\bar{X}$ by Q, x is repeated Q-times over a given symbol period, which is given by:

$$x_n = x_{n+Q} = x_{n+2Q}, =\ldots, = x_{n+(Q-1).Q}. \tag{6}$$

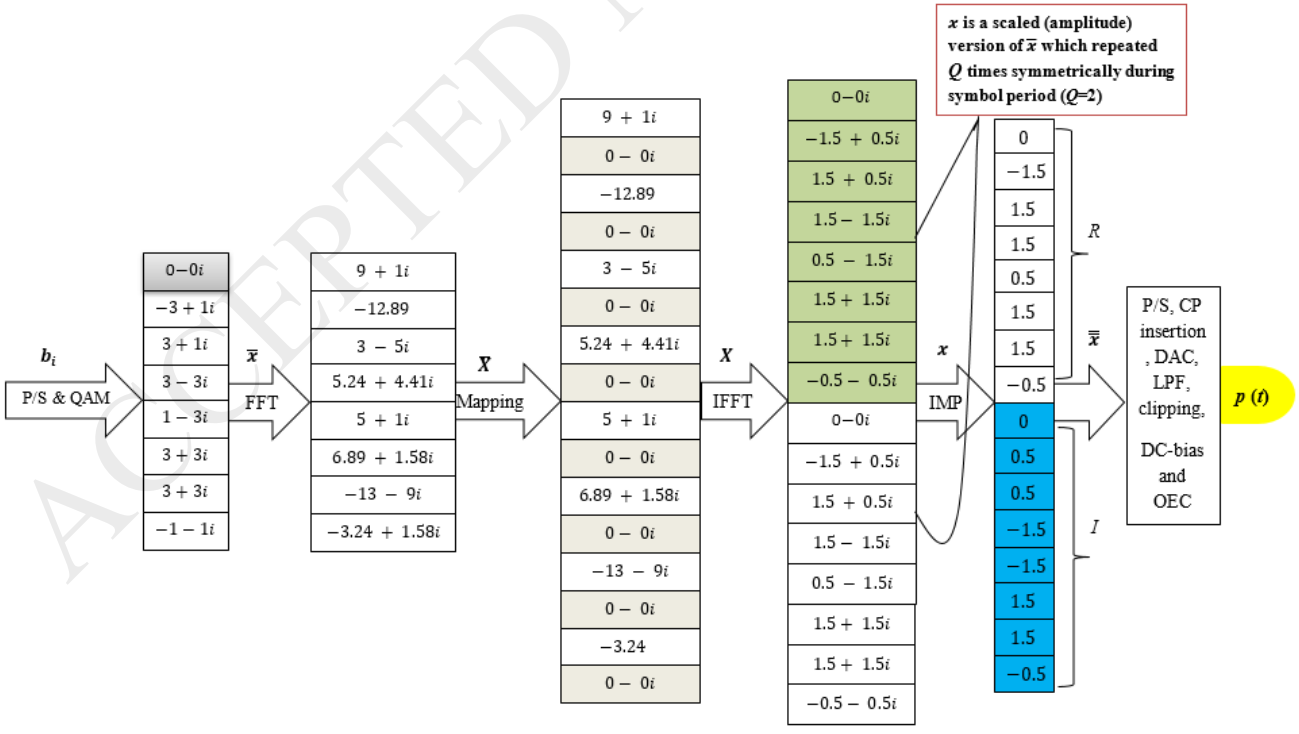

Fig. 1 Practical example of the OSC-IFDM Tx signal processing procedure

To make SC-IFDMA suitable for IM/DD VLC systems, the IMP block is inserted following the IFFT process. The IMP block consists of the following

two procedures: (*i*) removing the imaginary part of the first half of the SC-IFDMA symbol; and (*ii*) removing the real part of the second half of the SC-IFDMA symbol. Because of the symmetrical characteristic of x, this process does not result in any loss of information. The time domain real bipolar output samples of the IMP block are then transmitted using two sub-symbols [R, I], which are given by:

$$R = \begin{cases} \text{real } x_n, & \text{for } (n \le M-1) \\ 0 & otherwise \end{cases}, \tag{7}$$

$$I = \begin{cases} \text{imag } x_n, & \text{for } (M \le n < 2M) \\ 0 & otherwise \end{cases}. \tag{8}$$

Finally, the combined vector of these sub-symbols ($\bar{\bar{x}}$) is passed through a parallel to serial (P/S) converter, cyclic prefix (CP) insertion, digital to analogue converter (DAC), low pass filter (LPF) and clipping modules, followed by DC-biasing prior to the intensity modulation of the light source (i.e., electrical-to-optical conversion (EOC)). Note that, OSC-IFDM is a real bipolar scheme, which has almost the same low PAPR and high spectral efficiency as that of SC-IFDMA and DCO-OFDM, respectively.

2.2. OSC-IFDM receiver

Fig. 2 shows the block diagram of the OSC-IFDM Rx, which has the opposite functionality to that of the Tx. First, the photodetector (PD) converts the optical signal to an electrical signal $r(t)$, where $r(t) = R_i p(t) * h(t)$, R_i is the responsivity of the PD , $h(t)$ is the channel impulse response and * denotes the linear convolution operation. $r(t)$ is affected by the shot noise and thermal noise, which can be modeled as an additive white Gaussian noise (AWGN). The LPF, analogue to digital converter (ADC) and CP removal blocks are applied at the Rx. The resulting digital signal *yc* is subsequently fed into the IDMP block. Here, the original complex and repeated samples are reconstructed (i.e., x is convoluted with the chanel impulse response and added to AWGN) and passed through the FFT and equalizer blocks.

Two processes are carried out in the equalizer block, which are; *i*) de-interleaving mapping, where the un-modulated subcarriers are removed; and *ii*) compensation of channel effects by implementing a zero-forcing equalizer. Finally, the equalized digital signal (YC) passes through the IFFT, symbols estimator, QAM de-mapping and P/S blocks to reconstruct the information bits. The symbols estimator process is used to estimate the symbols prior to being affected by the DC-Bias.

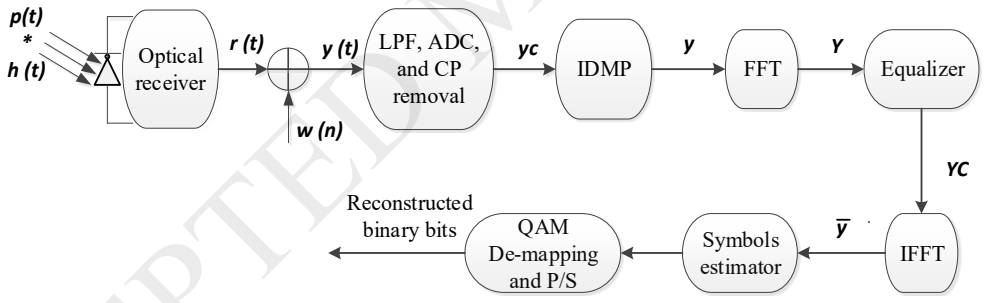

Fig. 2 Block diagram of the OSC-IFDM Rx

3. DC-Bias noise reduction algorithm

As the DC wandering and flickering interference of fluorescent lights affect the system performance at only the low frequency of the used bandwidth (i.e., < 15.625 KHz) [1], and as each OFDM subcarrier bandwidth is < 15.625 KHz (see Table 1), the first OFDM subcarrier will be negatively affected by the DC-bias, which subsequently can affect all OFDM samples in the time domain. This issue has been addressed in DCO-OFDM by un-modulating the first DCO-OFDM subcarrier (i.e., setting the first DCO-OFDM subcarrier to be zero). However, due to the implementation of the FFT at the OSC-IFDM Tx, the first OSC-IFDM subcarrier is a modulated subcarrier (i.e., not zero), see Fig. 1. Therefore, to overcome this problem, the first OSC-IFDM symbol is set to zero and the DC-bias noise reduction algorithm is introduced, which can be described as follows:

Referring to the block diagram of the OSC-IFDM Tx, the output vector of the IFFT process $x = [x_0, x_1, x_2 \ldots\ldots x_{N-1}]$, and x_n, as defined in (4) can be written as:

$$x_n = \frac{1}{N}\sum_{i=0}^{N-1} X_i \, e^{j2\Pi\frac{i}{N}n},$$

$$x_n = \frac{X_0 e^{j0}}{N} + \frac{1}{N}\sum_{i=1}^{N-1} X_i \; e^{j2\Pi \frac{i}{N} n.}$$

$$x_n = \left(\frac{1}{N}\sum_{i=1}^{N-1} X_i \; e^{j2\Pi \frac{i}{N} n.}\right) + \frac{X_0}{N}. \quad (9)$$

As already explained in subsection 2.1, setting the first OSC-IFDM symbol to zero (i.e., $\bar{x}_0 = 0$) also results in the first time domain sample being zero (i.e., $x_0 = 0$), see (5) and Fig. 1). As such, for $n = 0$, (9) can be re-written as:

$$x_0 = \left(\frac{1}{N}\sum_{i=1}^{N-1} X_i \; e^{j2\Pi \frac{i}{N} 0.}\right) + \frac{X_0}{N}$$

$$0 = \frac{1}{N}\sum_{i=1}^{N-1} X_i \; - \frac{X_0}{N}$$

$$X_0 = \sum_{i=1}^{N-1} X_i \quad (10)$$

From (10), X_0 can be easily reconstructed and therefore the effect of the DC wandering, and the fluorescent lights can be reduced in OSC-IFDM. However, the accuracy of this algorithm may be affected by the AWGN, as will be discussed in the results section (see Fig 5).

4. Simulation results

In this simulation study, a 256 points IFFT and 16-QAM were considered. All simulation parameters used in this study are listed in Table 1.

Table 1 – Simulation parameters

Parameter	Value
Number of OFDM time domain symbols	1000000
CP duration	50 ns [18]
Transmitter-receiver distance	100 cm
Bitrate	8 Mbps
Transmitter	
LED Type	OSRAM, SFH 4230 [12]
LED bandwidth	4 MHz
Subcarrier bandwidth	15.625 KHz
LED turn-on voltage (V_{on})	3 V
LED turn off voltage (V_{off})	4 V
LED linearity	1 V
DC bias value	3.5 V
Receiver	
PD type	Thorlab (PDA36A-EC)
PD bandwidth	10 MHz
PD gain	3 dB
PD responsivity	0.6
PD active area	15 mm^2
Receiver field of view (FOV) (full)	180^0

The results of the complementary cumulative distribution function (CCDF) vs. the PAPR relationship for DCO-OFDM and OSC-IFDM are compared in Fig. 3, where the PAPR comparisons were carried out for CCDF of 10^{-4} (i.e., $\Pr\{\text{PAPR} > PAPR_0\} = 0.0001$). From Fig. 3 it can be seen that, the PAPR of the proposed scheme is lower by 10 dB compared to the traditional DCO-OFDM scheme. This significant improvement is due to the implementation of the FFT and interleaving mapping processes before the implementation of the IFFT process, which makes the PAPR of OSC-IFDM as low as that of the SC-IFDMA scheme.

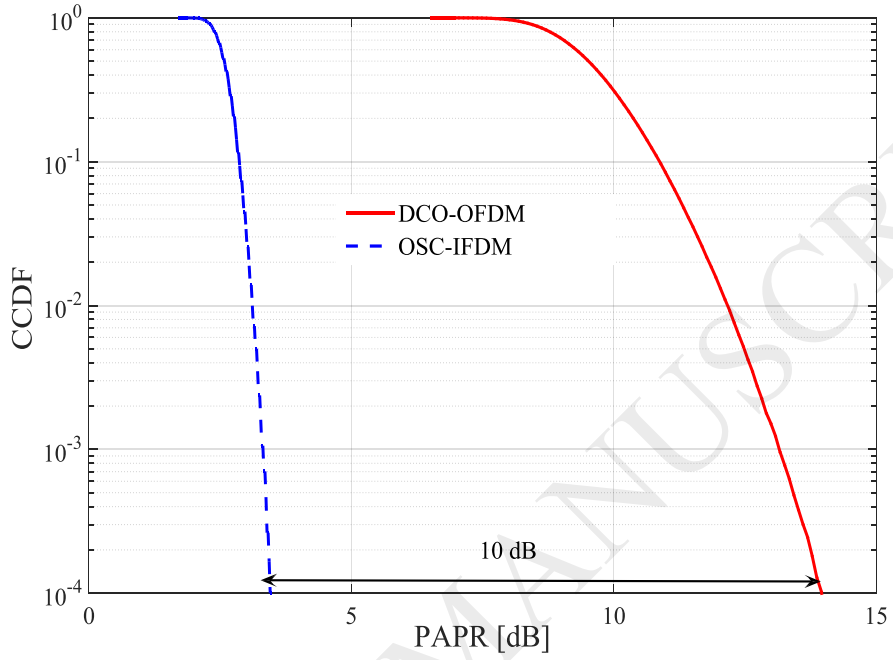

Fig. 3 CCDF vs. PAPR for the DCO-OFDM and OSC-IFDM schemes

The BER performance of both schemes (i.e., DCO-OFDM and OSC-IFDM) are simulated and compared as shown in Figs. 4 and 5. Note, the quantization, clipping, shot, terminal and DC wandering noise sources are due to the limited dynamic range of ADC and LED, photocurrent fluctuations, receiver electronics and LED bias, respectively. Here we have assumed that, both the shot noise and the terminal noise are modelled as AWGN [1].

Fig. 4 shows the BER performance as a function of the DAC dynamic range (DACDR) for the DCO-OFDM and OSC-IFDM schemes, where only the quantization noise is considered. In order to characterize the effect of the quantization noise only, no other noises were considered in the simulations. The transmission signal power was fixed at 10 dBm and DACDR=$20\log(2^c - 1)$ in dB [18], where c is the DAC bit resolution (e.g., the universal software radio peripheral (USRP) N210 has a DAC of 16 bits resolution [19]). From Fig. 4 it can be seen that, the BER performance of both schemes improves by increasing the DACDR. This is because the quantization level increases by c, but at the cost of the additional memory space. However, both schemes reach the noise floor (i.e., at a BER of 10^{-6}) at different DACDR levels, where the traditional DCO-OFDM and OSC-IFDM schemes require ~26 and ~13 dB of DACDR, respectively. Since the most practical DAC has a high DACDR of > 24 dB (e.g., for USRP N210 DACDR is 83 dB [19]), we determined that DACDR has a very limited effect on the system performance and therefore it is not considered in the subsequent analysis.

Fig. 5 plots the BER performance as a function of the average transmitted electrical signal power P_{avg} for the two schemes. We have used an OSRAM SFH 4230 LED [12] with the turn on voltage V_{on} and turn off voltage V_{off} of 3 and 4 V, respectively (i.e., biasing the LED at 3.5 V provides a 1 V peak-to-peak quasi-linear range). Therefore, to avoid the clipping noise, the peak-to-peak amplitude of the modulated transmitted electrical signal A_s must be swing between this value (i.e., $A_s \geq 1$ V). P_{avg} for both schemes were varied from 0 to 26 dBm and the noise power σ_n^2 was set to -10 dBm. As such, the SNR range was from 10 to 36 dB, which is within the reported SNR values for indoor VLC systems [1, 12]. Despite the fact that, the OSC-IFDM scheme uses the DC-bias reduction algorithm to remove the effect of low frequency noise, the results in this figure show that at P_{avg} < 21 dBm (i.e., SNR < 31 dB), the traditional DCO-OFDM scheme outperforms the OSC-IFDM scheme, due to the accuracy of the DC-bias noise reduction algorithm being affected by the AWGN. However, as both schemes have different PAPR rates (see Fig. 3), increasing SNR for both schemes (i.e., increasing P_{avg}) leads to reaching the threshold clipping. Therefore, and as illustrated in the same figure for $P_{avg} \geq 21$ dBm, the OSC-IFDM scheme outperforms the traditional DCO-OFDM scheme, as the BER performance of the latter is affected by the clipping noise for $P_{avg} = 21$ dBm, while the BER performance of the former starts is affected by the same noise source for P_{avg} =24 dBm (i.e., OSC-IFDM offers 3 dBm more P_{avg} compared to DCO-OFDM).

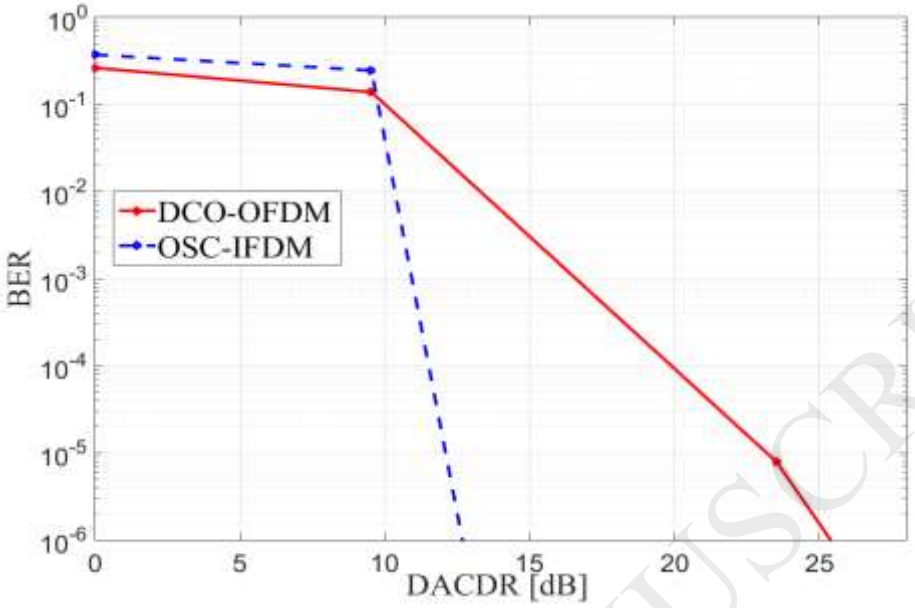

Fig. 4 DACDR vs. BER for DCO-OFDM and OSC-IFDM when only considering the quantization noise

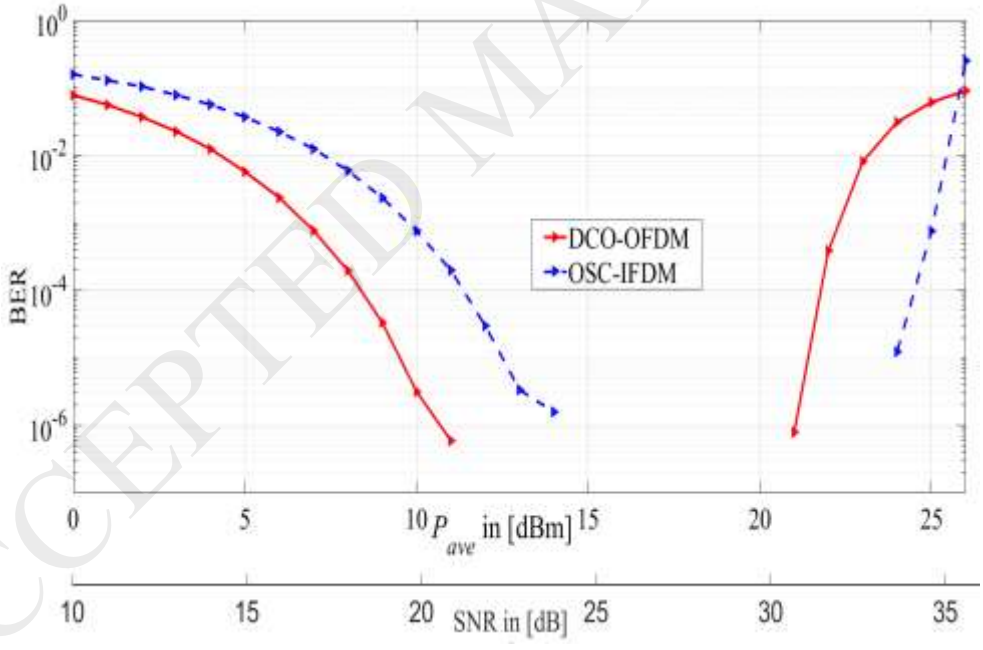

Fig. 5 The BER performance as a function of P_{avg} for DCO-OFDM and OSC-IFDM for a LED with 1 V limited dynamic range. P_{avg} of both schemes varied from 0 to 26 dBm and the noise power σ_n^2 was set to -10 dBm (as such, the SNR range was from 10 dB to 36 dB)

5. Conclusion

In this paper, the symmetrical time domain characteristics of SC-IFDMA were exploited for the intensity modulation and direct detection VLC system applications by symmetrically repeating the SC-IFDMA time domain samples twice during each SC-IFDMA time domain symbol period. This was achieved by setting the interleaving mapping factor at the frequency domain to 2. Simulation of the OSC-IFDM scheme were conducted demonstrating that the PAPR

value of the proposed scheme is 10 dB lower than that of the DCO-OFDM scheme. The impact of the reduced PAPR on the system performance was also simulated while considering the effect of the dynamic range of the digital-to-analogue converter and the LED. The results showed that the DACDR performance is enhanced by almost 14 dB for OSC-IFDM compared to DCO-OFDM. Furthermore, when considering the dynamic range of the LED, the results showed that OSC-IFDM provided 3 dBm more average power in comparison to DCO-OFDM. However, the simulation results showed that with no clipping noise, DCO-OFDM outperforms OSC-IFDM. This is due to the effects of the low-frequency noise, which only impacts OSC-IFDM since its first subcarrier is modulated.

Acknowledgements

The first author acknowledges and greatly appreciates the financial support received from the Ministry of Education in Libya and the University of Gharyan. This work was supported by the UK EPSRC grant EP/P006280/1: Multifunctional Polymer Light-Emitting Diodes with Visible Light Communications (MARVEL), and the European Union Horizon 2020 research and innovation programme under the Marie Sklodowska-Curie grant agreement no 764461 (VISION).

Reference

[1] Z. Ghassemlooy, W. Popoola, and S. Rajbhandari, *Optical wireless communications: system and channel modelling with Matlab, 2nd Edition*. CRC Press, 2019.

[2] Z. Ghassemlooy, L. N. Alves, S. Zvanovec, and M-A. Khalighi, *Visible Light Communications*: Theory and Applications, CRC Press, June 2017.

[3] O. Saied, Z. Ghassemlooy, X. Tang, X. Dai, H. Le Minh, and B. Lin, "Position encoded asymmetrically clipped optical orthogonal frequency division multiplexing in visible light communications," *Journal of Communications and Information Networks,* vol. 2, no. 4, pp. 1-10, 2017.

[4] S.-W. Wang *et al.*, "A high-performance blue filter for a white-led-based visible light communication system," *IEEE wireless communications,* vol. 22, no. 2, pp. 61-67, 2015.

[5] S. Rajbhandari *et al.*, "A review of gallium nitride LEDs for multi-gigabit-per-second visible light data communications," *Semiconductor Science and Technology,* vol. 32, no. 2, p. 023001, 2017.

[6] P. A. Haigh, Z. Ghassemlooy, S. Rajbhandari, I. Papakonstantinou, and W. Popoola, "Visible light communications: 170 Mb/s using an artificial neural network equalizer in a low bandwidth white light configuration," *Journal of lightwave technology,* vol. 32, no. 9, pp. 1807-1813, 2014.

[7] H. Chun *et al.*, "LED based wavelength division multiplexed 10 Gb/s visible light communications," *Journal of lightwave technology,* vol. 34, no. 13, pp. 3047-3052, 2016.

[8] O. Saied *et al.*, "Pilot-aided asymmetrically clipped optical OFDM in visible light communication," *The Mediterranean journal of electronics and communications,* vol. 12, no. 2, pp. 64-71, 2016.

[9] S. D. Dissanayake and J. Armstrong, "Comparison of ACO-OFDM, DCO-OFDM and ADO-OFDM in IM/DD systems," *Journal of lightwave technology,* vol. 31, no. 7, pp. 1063-1072, 2013.

[10] L. C. Mathias, L. F. De Melo, and T. Abrao, "3-D Localization With Multiple LEDs Lamps in OFDM-VLC System," *IEEE Access,* vol. 7, pp. 6249-6261, 2019.

[11] C. R. Berger, Y. Benlachtar, and R. Killey, "Optimum clipping for optical OFDM with limited resolution DAC/ADC," in *Signal Processing in Photonic Communications*, 2011, p. SPMB5: Optical Society of America.

[12] R. Mesleh, "OFDM and SCFDE performance comparison for indoor optical wireless communication systems," in *19th International Conference on Telecommunications (ICT)*, 2012, pp. 1-5: IEEE.

[13] K. Acolatse, Y. Bar-Ness, and S. K. Wilson, "Single carrier frequency domain equalization for optical wireless communications."

[14] C. Wu, H. Zhang, and W. Xu, "On visible light communication using LED array with DFT-spread OFDM," in *IEEE International Conference on Communications (ICC)*, 2014, pp. 3325-3330: IEEE.

[15] O. Saied *et al.*, "Single carrier optical FDM in visible light communication," in *10th International Symposium on Communication Systems, Networks and Digital Signal Processing (CSNDSP)*, 2016, pp. 1-5: IEEE.

[16] D. Tsonev, S. Sinanović, and H. Haas, "Pulse shaping in unipolar OFDM-based modulation schemes," in *IEEE Globecom Workshops*, 2012, pp. 1208-1212: IEEE.

[17] H. G. Myung, L. Junsung, and D. Goodman, "Peak-To-Average Power Ratio of Single Carrier FDMA Signals with Pulse Shaping," in *Personal, Indoor and Mobile Radio Communications, 2006 IEEE 17th International Symposium on*, 2006, pp. 1-5.

[18] J. Garcia, S. G. LaJeunesse, and D. Bartow, "Measuring spurious free dynamic range in a D/A converter," *Intersil Technical Brief,* pp. 1-2, 1995.

[19] Ettus.Research. (2014). *USRP™ N200/N210 networked series*. Available: https://www.ettus.com/content/files/07495_Ettus_N200-210_DS_Flyer_HR_1.pdf